# Near-Infrared Light Propagation in an Adult Head Model with Refractive Index Mismatch

Seunghwan Kim and Jae Hoon Lee

**We investigate near-infrared light (NIR) propagation in a model of an adult head using an extensive Monte Carlo (MC) simulation. The adult head model is a four-layered slab which consists of a surface layer, a cerebrospinal fluid layer, a gray-matter layer, and a white-matter layer. We study the effects of a refractive index mismatch on the model, calculating the intensity of detected light, mean flight time, and partial mean flight time of each layer for various refractive indices of the cerebrospinal fluid layer as functions of source-detector spacing. The Monte Carlo simulation shows that the refractive index mismatch presents very rich results including rapidly decaying intensity of detected light and a peak and cross-over in the partial mean flight time with source-detector spacing. We also investigate spatial sensitivity profiles at various source-detector spacings, discussing the index mismatch effect on the model.**

**Keywords: Light propagation, head model, refractive index.**

Manuscript received May 11, 2004; revised May 30, 2005.

This work was supported by the Ministry of Information and Communication of Korea.

Seunghwan Kim (phone: +82 42 860 5465, email: skim@etri.re.kr) and Jae Hoon Lee (email: ljh63452@etri.re.kr) are with Basic Research Laboratory, ETRI, Daejeon, Korea.

## I. Introduction

In the last decade, the study of light propagation through strongly scattering media has received increasing attention as a result of the application of a near-infrared (NIR) diffusing-light probe to biomedical investigations such as blood oximetry [1]-[3], the noninvasive measurement of tissue oxygenation in the brain [4]-[8], and direct imaging of breast tumors [9]-[11]. Biological tissues are classified as turbid media because their absorption coefficients are negligible compared with their scattering coefficients [12]. Since most propagating photons in biological tissues experience a large number of scattering events before they finally are absorbed or emerge from tissues through interfaces, the NIR light propagation in biological tissues is described very well by diffusion approximation [13]-[15]. Many studies [16]-[20] have been performed using diffusion approximation.

Specifically, a great deal of research has been motivated by the ability of optical radiation to diagnose brain tumors. However, a problem arises in studying complex systems such as the brain, in which not all regions diffuse light. In the brain, there is a clear region composed with cerebrospinal fluid (CSF), in which both of the scattering and absorption coefficients are negligible. The diffusion approximation no longer holds in the clear region. To solve the problem, some approximations such as a hybrid radiosity-diffusion theory have been suggested [21]-[23].

Recently, in a variety of models of the adult head, the effects of both the presence of the surface tissues including a clear CSF layer around the brain and the brain anatomy itself have been investigated [24]. By the experiment and the Monte Carlo (MC) and finite-element calculations in [24], the authors concluded that the clear CSF layer significantly affects light

propagation in the adult head once the spacing between the source and detector is large. Although many studies on light propagation in a head model have been published, the effects of the refractive index (RI) mismatch in a head model have not been considered. The RI is an optical property which leads to important effects on light propagation at interfaces [25].

In this paper, we investigate NIR light propagation in a model of the adult head by extensive MC simulation considering the RI mismatch. The adult head model is a four-layered slab which consists of a surface layer, a CSF layer, a gray-matter (GM) layer, and a white-matter (WM) layer. The model was also considered by Okada and others in [24]. We study the effect of an RI mismatch on a model, calculating the intensity of detected light, mean flight time (MFT), and partial mean flight time (PMFT) of each layer for various RIs of the CSF layer as functions of source-detector (SD) spacing. The PMFT calculated in this paper is the MFT that the detected light has spent in a particular layer. The MC simulation shows that the RI mismatch presents very rich results including rapidly decaying intensity of detected light and a peak and cross-over of the PMFT as a function of SD spacing. We also investigate spatial sensitivity profiles (SSPs) deduced from the accumulated optical path histories of the photons reaching the detector, and discuss the RI mismatch effect on the model at various spacings.

In sections II and III, we introduce the adult head model and MC simulation method considered, respectively. Section IV shows the results of the extensive MC simulation for the model with various RIs of CSF. We conclude in section V with our summarized results.

## II. Adult Head Model

Many adult head models ranging from a three-layered slab [24] to a circular four-layered model with a block intrusion [26] have been studied. Okada and others [24] studied NIR light propagation in various models such as a three-layered slab without a CSF layer, four-layered slab with a CSF layer, four-layered slab with uneven boundary between the GM and the WM, and four-layered slab with slots imitating the sulci filled with CSF. They concluded that a CSF layer significantly affects light propagation in an adult head, but the geometries of the sulci and the boundary between the GM layer and the WM layer scarcely affect the optical path.

Dehghani and Delpy [26] studied the effects of obstruction in a CSF layer on light distribution in tissue with a circular four-layered model. They concluded that the sensitivity of the NIR light signal to the deeper tissues is not greatly improved even with the introduction of intrusions that completely span the CSF layer. However, the sensitivity of the signal to absorption changes in the intrusion itself is considerably increased together with that of the tissues immediately adjacent to the intrusion.

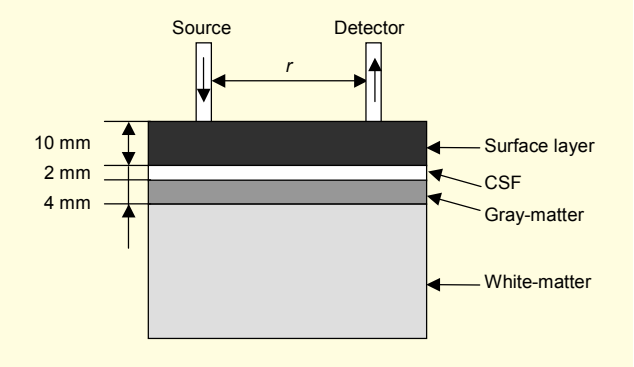


Fig. 1. Schematic design of an adult head model.

In this paper, we investigate the effects of an RI mismatch between the tissues on NIR light propagation in an adult head. To focus on the effects of the RI mismatch, we chose a simple adult head model consisting of four different homogeneous media including a surface layer, a CSF layer, a GM layer, and a WM layer. The surface layer imitates the scalp and skull. The thickness of each layer is 10 mm, 2 mm, 4 mm, and semi-infinite, respectively. To study the effects of the RI mismatch between the tissues, we considered a model with various RIs of CSF ranging from 1.0 to 1.8 and RIs of the other tissues at 1.4. The geometries and optical properties for each layer of the model are shown in Fig. 1 and Table 1, respectively. The geometries and optical properties have been chosen from the reported data on the optical properties of the tissues [12], [27], and [28].

Table 1. Optical properties of the tissues in the adult head model given by Fig. 1.

| Tissue type | $\mu_s$ ($mm^{-1}$) | $\mu_a$ ($mm^{-1}$) | $n$ | $g$ |
|---|---|---|---|---|
| scalp & skull | 20 | 0.04 | 1.4 | 0.9 |
| CSF | 0 | 0 | 1.0 - 1.8 | 0 |
| GM | 25 | 0.025 | 1.4 | 0.9 |
| WM | 60 | 0.005 | 1.4 | 0.9 |

$\mu_s$: scattering coefficients, $\mu_a$: absorption coefficient, n: refractive index, g: scattering anisotropy factor.

## III. Monte Carlo Simulation

In this study, we used the MC algorithm for light transport in the multi-layered tissues described in [29] and [30]. The MC algorithm describes the local rules of photon propagation, which are expressed as probability distributions describing the step size of photon movement between sites of photon-tissue

interaction and the angles of deflection in a photon's trajectory when a scattering event occurs. In the simulation, we calculated the intensity, MFT, and PMFT in each layer of detected light as functions of SD spacing. In the simulation, the number of photons ranges from a half billion to one billion.

Figure 2 shows a flowchart of the MC algorithm for the multi-layered tissues. The flowchart begins with a question that asks whether or not the photon is in the CSF layer. Since there is no scattering in the CSF layer, the photon in the layer moves to the boundary of the layer without a scattering event.

The RI mismatch at the boundaries of the CSF layer affects the transmission angle and the internal reflectance at the boundaries leading to the rich behaviors of the MFT of detected light as a function of SD spacing. The transmission angle and the internal reflectance at the boundary are determined by Snell's law (1) and Fresnel's formula (2), respectively. Snell's law (1) indicates the relationship between the angle of incidence, $\theta_i$, the angle of transmission, $\theta_t$, and the RIs of the media that the photon is incident from, $n_i$, and transmitted to, $n_t$. Fresnel's formula (2) presents the internal reflectance $R$ as an average of the reflectances for the two orthogonal polarization directions.

$$n_i \sin\theta_i = n_t \sin\theta_t \tag{1}$$

$$R = \frac{1}{2}\left[\frac{\sin^2(\theta_i - \theta_t)}{\sin^2(\theta_i + \theta_t)} + \frac{\tan^2(\theta_i - \theta_t)}{\tan^2(\theta_i + \theta_t)}\right] \tag{2}$$

The internal reflection is used for describing the reflection of the beam impinging from a higher RI medium. In the case of a higher CSF's RI than that of other regions, the internal reflection has to be considered for the beam impinging from the CSF to other regions. In the case of a lower CSF's RI than that of other regions, the internal reflection has to be considered for the beam impinging from other regions to the CSF.

In the simulation, the RI mismatch between the surface layer and air surrounding it, as well as the RI mismatch between the CSF layer and the other tissues, are considered.

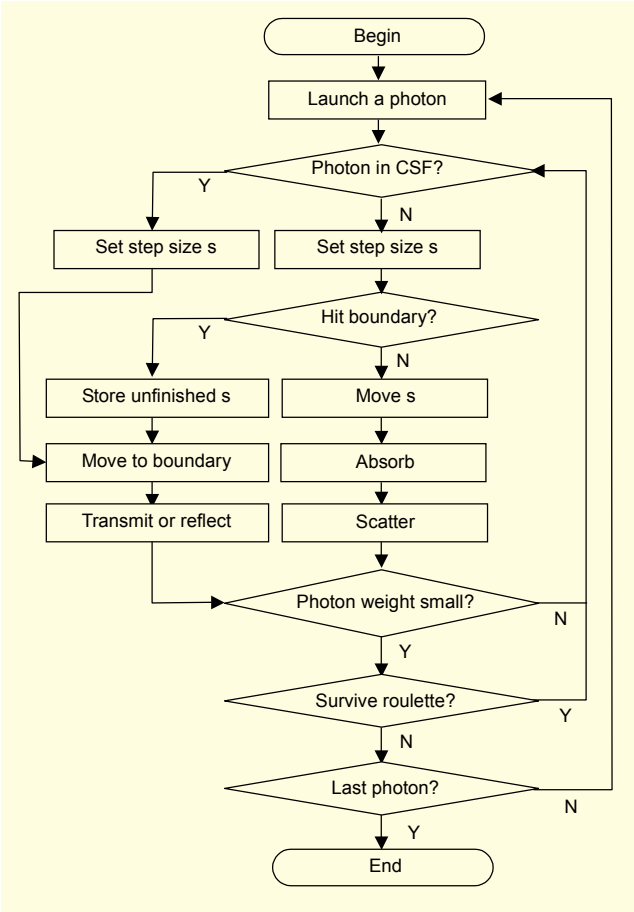


Fig. 2. Flowchart of MC simulation for multi-layered tissues. s: the step size of photon movement between sites of photon-tissue interaction.

## IV. Results and Discussion

### 1. Detected Light Intensity and Mean Flight Time

Figure 3 shows the intensity of detected light, $I$, normalized by the source intensity as a function of SD spacing, $r$, for various RIs of the CSF layer, $n_{CSF}$. When there is no RI mismatch, that is, $n_{CSF} = 1.4$, the results shown in Fig. 3 are similar to those in [24]. Intensity $I(r)$ decreases as $r$ increases. For $r > r_c$, equal to approximately 20 mm, the rate of decline in $I(r)$ with $r$ diminishes, which comes from the role of the CSF layer discussed in [24]. Since there is no scattering and absorption in the CSF layer, the light can propagate farther through the CSF layer than in other tissues. Thus, the CSF layer plays the role of a light conduit. However, since the transmission from the CSF layer to other layers occurs, and vice versa, the CSF layer is not a waveguide. In the presence of the CSF layer, most of the light propagates through the CSF layer when the light meets it. Thus, the light penetrating into the brain is very small compared with that in the case of no CSF layer. Therefore, the head models with and without CSF layer give different results regardless of the early arriving strong signal.

When there is an RI mismatch, that is, $n_{CSF} \neq 1.4$, the results shown in Fig. 3 indicate that $I(r)$ is independent of $n_{CSF}$ for $r < r_c$. For $r > r_c$, the rate of decline in $I(r)$ with $r$ increases as the amount of the RI mismatch $|n_{CSF} - 1.4|$ increases. The increase of the rate of decline in $I(r)$ for $n_{CSF} < 1.4$ is smaller than that for $n_{CSF} > 1.4$. This implies that the RI mismatch affects the light propagation, reducing the role of the CSF layer

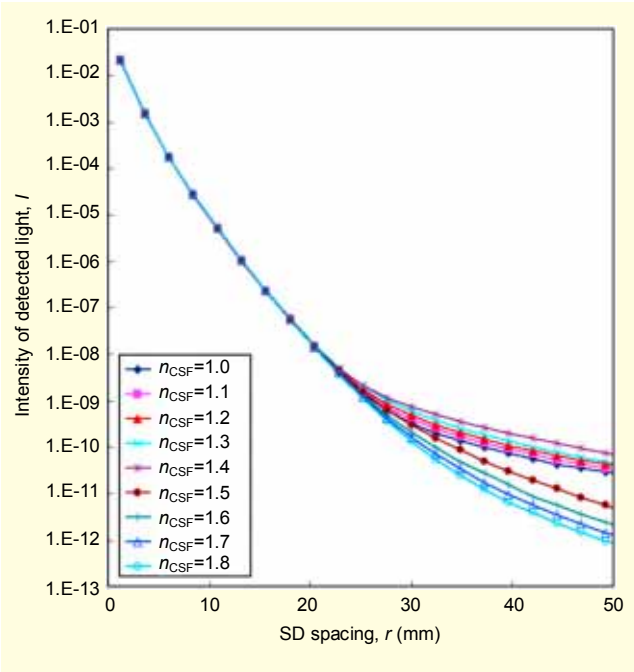


Fig. 3. Intensity of detected light, $I$, as a function of SD spacing, $r$, for various RIs of the CSF layer, $n_{CSF}$.

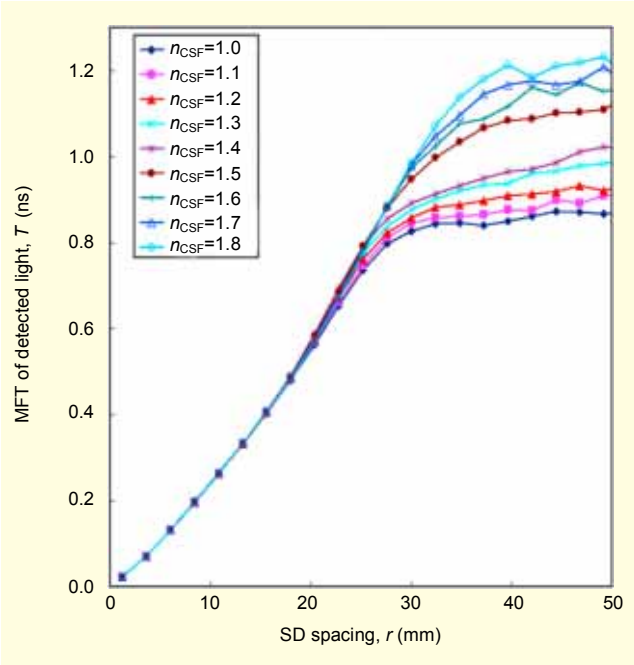


Fig. 4. MFT of detected light, $T$, as a function of SD spacing, $r$, for various RIs of the CSF layer, $n_{CSF}$.

as the conduit in the light propagation. The effect of the RI mismatch for $n_{CSF} > 1.4$ is larger than that for $n_{CSF} < 1.4$. For $n_{CSF} > 1.4$ the transmission angle is smaller than the incidence angle by Snell's law (1) when the light impinges from other regions to the CSF layer; thus, light cannot go farther through the CSF, enhancing the RI mismatch effect. For $n_{CSF} < 1.4$ the behavior reverses, reducing the RI mismatch effect.

Figure 4 shows the MFT of detected light, $T$, as a function of $r$ for various $n_{CSF}$. When $n_{CSF} = 1.4$, the results shown in Fig. 4. are similar to those in [24]. The MFT of detected light $T(r)$ increases as $r$ increases. For $r > r_c$ equal to approximately 20 mm, the rate of increase in $T(r)$ with $r$ diminishes, which comes from the role of the CSF layer as the conduit of light propagation. When $n_{CSF} \neq 1.4$, the results in Fig. 4 show that $T(r)$ is independent of $n_{CSF}$ for $r < r_c$. As $r$ increases for $r > r_c$, the rate of increase in $T(r)$ with $r$ diminishes quickly for the model with $n_{CSF} < 1.4$ and slowly for the model with $n_{CSF} > 1.4$. This implies that the larger $n_{CSF}$ is, the more time it takes for a photon to go by a distance larger than $r_c$. This behavior comes from the fact that the velocity of a photon in the CSF layer slows down by $c \cdot n_{CSF}^{-1/2}$ for $n_{CSF} > 1$, with light velocity $c$ at a vacuum.

## 2. Partial Mean Flight Time

Figure 5 shows the PMFT of detected light at the surface layer, $T_s$, as a function of $r$, for various $n_{CSF}$. When $n_{CSF} = 1.4$, the results in Fig. 5 are similar to those in [24]. As $r$ increases, $T(r)$ peaks at $r = r_p$, where $r_p$ is approximately 30 mm, beyond which $T(r)$ decreases very slowly. The peak did not appear in [24] because the simulation in [24] was not performed with enough photons to show the peak. The peak comes from the fact that the CSF layer plays a role as a conduit of light

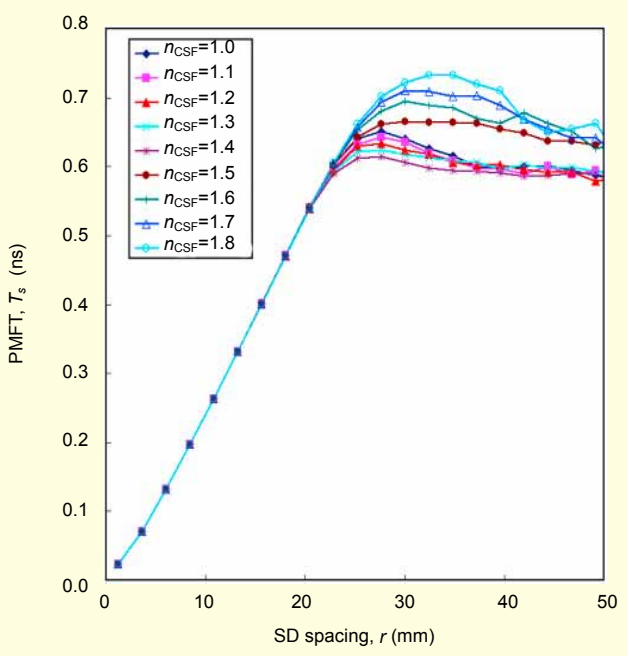


Fig. 5. PMFT of detected light at the surface layer, $T_s$, as a function of SD spacing, $r$, for various RIs of the CSF layer, $n_{CSF}$.

propagation. Since more resident time at the surface layer is needed to go farther, $T_s(r)$ increases as $r$ increases for a small $r$. Beyond $r_p$, at which the photon begins to enter the CSF layer, the photon goes farther through the CSF layer, leading to a decrease of $T_s(r)$. When $n_{CSF} \neq 1.4$, the results in Fig. 5 show that $r_p$ and $T_s(r_p)$ increase as the amount of the RI mismatch increases. Since the internal reflection $R$ given by (2) due to the RI mismatch reduces the role of the CSF layer as a conduit of light propagation, the behavior appears.

Figure 6 shows the PMFT of detected light at the CSF layer, $T_{CSF}$, as a function of $r$, for various $n_{CSF}$. When $n_{CSF} = 1.4$, the results shown in Fig. 6 are similar to those in [24]. The PMFT of detected light $T_{CSF}(r)$ is negligible for $r < r_a$ of approximately 15 mm. Beyond $r_a$, $T_{CSF}(r)$ increases as $r$ increases. This implies that photons begin to enter the CSF layer at $r = r_a$. Since photons go farther through the CSF layer, $T_{CSF}(r)$ increases as $r$ increases. When $n_{CSF} \neq 1.4$, the results in Fig. 6 show a similar behavior of $T_{CSF}(r)$ with $r$ to that for the case of $n_{CSF} = 1.4$. Detected light $T_{CSF}(r)$ is negligible for $r < r_a$. Beyond $r_a$, $T_{CSF}(r)$ increases as $r$ increases. The rate of increase of $T_{CSF}(r)$ with $r$ decreases as $n_{CSF}$ decreases from 1.4, leading to a smaller $T_{CSF}(r)$ for $n_{CSF} < 1.4$ than for $n_{CSF} = 1.4$. This behavior comes from the facts that the velocity of light in the CSF layer increases as $n_{CSF}$ decreases, leading to the decrease of $T_{CSF}(r)$, and that the internal reflectance $R$ increases as $n_{CSF}$ decreases from 1.4, reducing the role of the CSF layer as the conduit of light propagation and thus reducing $T_{CSF}(r)$. At an intermediate $r$, the rate of increase of $T_{CSF}(r)$ with $n_{CSF} > 1.4$ decreases as $r$ increases, leading to $T_{CSF}(r)$ with $n_{CSF} > 1.4$, which is less than $T_{CSF}(r)$ with $n_{CSF} = 1.4$. At a large $r$, the rate of increase of $T_{CSF}(r)$ with $n_{CSF} > 1.4$ increases as $r$ increases leading to $T_{CSF}(r)$ with $n_{CSF} > 1.4$, which is greater than $T_{CSF}(r)$ with $n_{CSF} = 1.4$. The crossing of $T_{CSF}(r)$ with $r$ for $n_{CSF} > 1.4$ comes from two competing factors: that the velocity of light in the CSF layer decreases as $n_{CSF}$ increases, leading to an increase of $T_{CSF}(r)$, and that the internal reflectance R increases as $n_{CSF}$ increases from 1.4, reducing the role of the CSF layer as the conduit of light propagation and thus reducing $T_{CSF}(r)$. Since the effect of the former increases as $r$ increases and the effect of the latter is uniform regardless of $r$, the latter dominates the former at an intermediate $r$, and the former dominates the latter at a large $r$.

Figure 7 shows the PMFT of detected light at the GM layer, $T_g$, as a function of $r$, for various values of $n_{CSF}$. When $n_{CSF} = 1.4$, the results in Fig. 7 are similar to those in [24]. The detected light $T_g(r)$ is negligible for $r < r_a$ of approximately 15 mm. Beyond $r_a$, $T_g(r)$ increases abruptly as $r$ increases up to $r_p$ of approximately 30 mm. Beyond $r_p$, $T_g(r)$ is saturated as a constant value. This implies that the photons begin to enter the GM at $r$ of approximately $r_a$, and go to the WM through the GM at $r$ of approximately $r_p$, leading to a uniform $T_g(r)$ for $r > r_p$. For $n_{CSF} < 1.4$, the results in Fig. 7 show a similar behavior of $T_g(r)$ with $r$ to that for the case of $n_{CSF} = 1.4$. Detected light $T_g(r)$ is negligible for $r < r_a$ of approximately 15 mm. Beyond $r_a$, $T_g(r)$ increases abruptly as $r$ increases up to $r = 30$ mm. Beyond $r_p$,

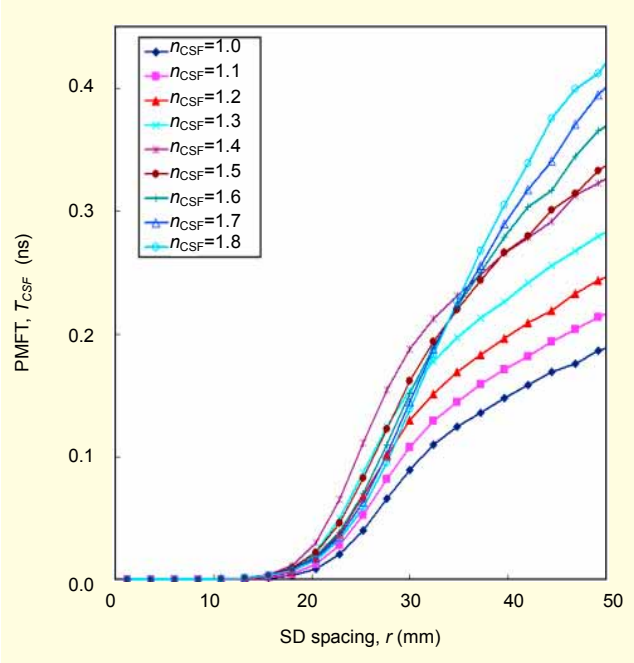


Fig. 6. PMFT of detected light at the CSF layer, $T_{CSF}$, as a function of SD spacing, $r$, for various RIs of the CSF layer, $n_{CSF}$.

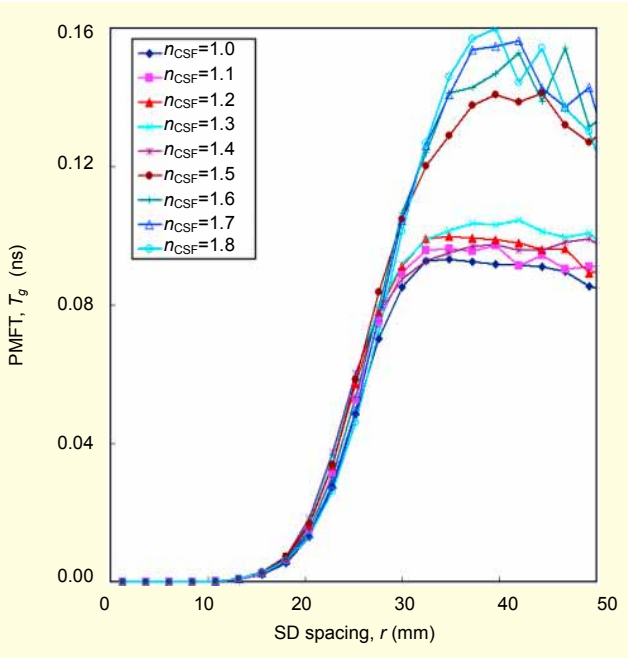


Fig. 7. PMFT of detected light at the GM layer, $T_g$, as a function of SD spacing, $r$, for various RIs of the CSF layer, $n_{CSF}$.

$T_g(r)$ is saturated as a constant value. For $n_{CSF} > 1.4$, the results in Fig. 7 show a different behavior of $T_g(r)$ with $r$ as that for the case of $n_{CSF} = 1.4$. Detected light $T_g(r)$ is negligible for $r < r_a$. Beyond $r_a$, $T_g(r)$ increases abruptly as $r$ increases up to $r = 37$ mm. Beyond $r_s$, $T_g(r)$ decreases as $r$ increases, leading to a peak at $r = r_s$. The existence of the peak implies that there is an appropriate SD spacing to investigate the change of optical properties of the GM provided $n_{CSF}$ is greater than 1.4.

Figure 8 shows the PMFT of detected light at the WM layer, $T_w$, as a function of $r$, for various $n_{CSF}$. The behavior of $T_w(r)$ with $r$ is similar to that of $T_g(r)$ with $r$ shown in Fig. 7. Detected light $T_w(r)$ is negligible for $r < r_a = 15$ mm. Beyond $r_a$, $T_w(r)$ increases abruptly as $r$ increases up to $r = 30$ mm for $n_{CSF} \le 1.4$ and up to $r = 37$ mm for $n_{CSF} > 1.4$. For $n_{CSF} \le 1.4$, $T_w(r)$ is saturated to a constant value as $r$ increases beyond $r_p$. For $n_{CSF} > 1.4$, $T_w(r)$ decreases as $r$ increases beyond $r_s$ leading to a peak at $r = r_s$. The existence of the peak implies that there is an appropriate SD spacing to investigate the change of optical properties of the WM provided $n_{CSF}$ is greater than 1.4.

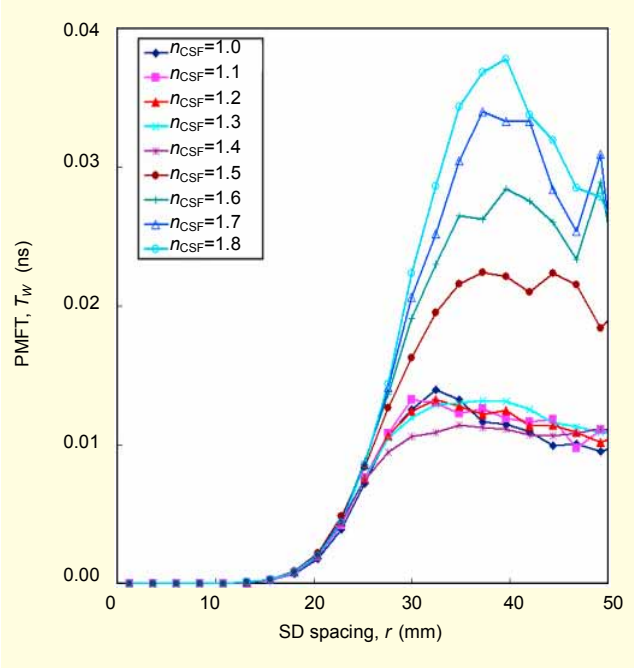


Fig. 8. PMFT of detected light at the WM layer, $T_w$, as a function of SD spacing, $r$, for various RIs of the CSF layer, $n_{CSF}$.

### 3. Spatial Sensitivity Profiles

Figure 9 shows the SSPs for the models with various RIs of the CSF layer at SD spacing $r$ ranging from 1.2 to 44.4 mm. In Fig. 9, the SSPs are confined to the surface layer for a small $r$. For an intermediate $r$, the SSPs spread farther toward the clear CSF and GM layers, and very little light reaches the WM layer. For a large $r$, the SSPs have shifted toward the deeper layers

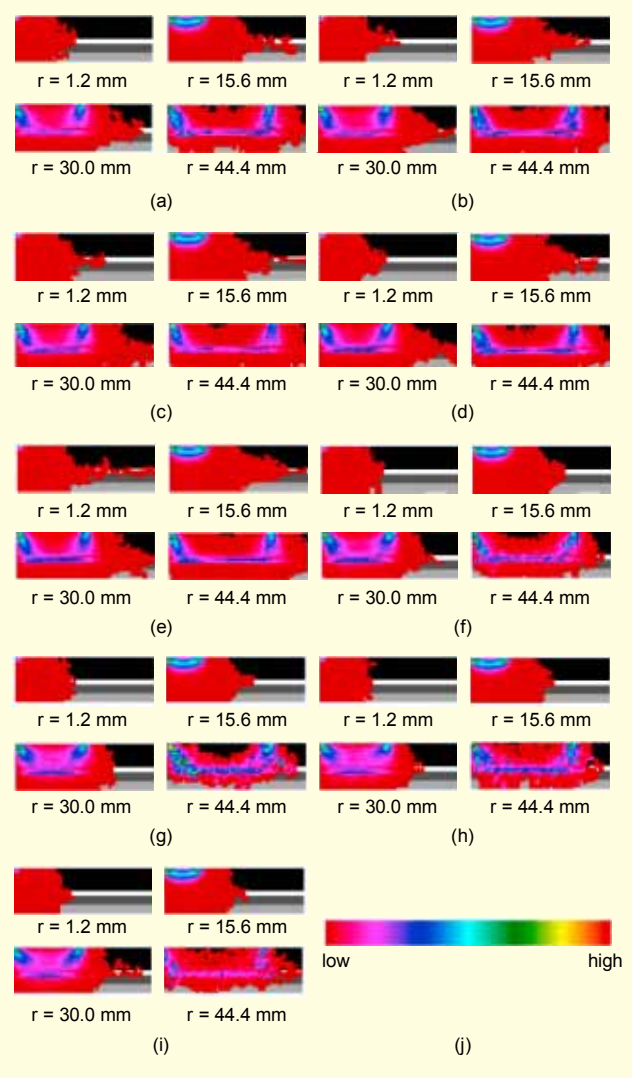


Fig. 9. The SSPs for the models with the RIs of the CSF layer: (a) $n_{CSF} = 1.0$, (b) $n_{CSF} = 1.1$, (c) $n_{CSF} = 1.2$, (d) $n_{CSF} = 1.3$, (e) $n_{CSF} = 1.4$, (f) $n_{CSF} = 1.5$, (g) $n_{CSF} = 1.6$, (h) $n_{CSF} = 1.7$, and (i) $n_{CSF} = 1.8$ at SD spacings, $r = 1.2$ mm, 15.6 mm, 30.0 mm, and 44.4 mm, with (j) as a color map for the figures.

and an apparent light path can be seen around the clear CSF layer. However, the detected light still does not tend to penetrate into the WM layer. Figure 9 does not show the dependence of the SSPs on the RIs of the CSF layer due to the insufficient information of the SSPs on the RI mismatch effect.

## V. Conclusion

In this study, we performed an extensive MC simulation of light propagation for an adult head model investigating the effects of an RI mismatch at the boundaries of the CSF layer. The MC simulation shows that the RI mismatch presents a very rich behavior of the detected light intensity, the MFT of photons, and the PMFT of photons as functions of SD spacing.

The rate of decline in the detected light intensity with the spacing increases as the amount of the RI mismatch increases for a large SD spacing. The rate of increase in the MFT with the spacing diminishes quickly for the model with a small RI of the CSF layer and slowly for the model with a large RI of the CSF layer as the spacing increases. A peak appears in the PMFT of detected light at the surface layer with the spacing. Both the position and value of the peak increase as the amount of the RI mismatch increases. The rate of increase of the PMFT at the CSF layer with the spacing decreases for a large spacing as the RI of the CSF layer decreases from the matched RI of the CSF layer. As the RI of the CSF layer increases from the matched RI of the CSF layer, the rate of increase of the PMFT at the CSF layer with the spacing decreases for the intermediate spacing and increases for the large spacing, showing the crossing of the PMFT at the CSF layer by the large and small RIs of the CSF layer. A peak appears in the PMFT of the GM layer and the WM layer for the large RI of the CSF layer.

The rich behavior of the detected light intensity, the MFT of photons, and the PMFT of photons at each layer with the spacing comes from the role of the CSF layer as a conduit of light propagation and the effect of the RI mismatch at the boundaries of the CSF layer. The RI mismatch affects light propagation, reducing the role of the CSF layer as a conduit by the internal reflection. The CSF layer with greater RI shows a larger RI mismatch effect than that of the CSF layer with a smaller RI.

In conclusion, the RI mismatch of the CSF layer has to be considered to investigate the change of the optical properties of the brain. In particular, there is an appropriate SD spacing to investigate the change of the optical properties of the brain when the RI of the CSF layer is larger than the matched RI of the CSF layer. The range of the CSF's RI considered in this study is broader than that of the real CSF's RI. We extended the range of the CSF's RI to maximize the RI mismatch effect on light propagation. Although the range of the CSF's RI is broader than the real CSF's RI, the tendency of the RI mismatch effect and the various behaviors of light propagation may be preserved in a real head. For a more realistic study, we have to research a more realistic head model considering the shape of the skull and brain, the RI mismatch of the other tissues, and so on.

## References


[1] R.N. Pittman, "In Vivo Photometric Analysis of Hemoglobin," *Ann. Biomed. Eng.*, vol. 14, no. 2, 1986, pp. 119-137.

[2] J.M. Schmitt, "Simple Photon Diffusion Analysis of the Effects of Multiple Scattering on Pulse Oximetry," *IEEE Trans. Biomed. Eng.*, vol. 38, no. 12, Dec. 1991, pp. 1194-1203.

[3] V. Ntziachristos, M. Kohl, H. Ma, and B. Chance, "Oximetry Based on Diffuse Photon Density Wave Differentials," *Med. Phys.*, vol. 27, no. 2, Feb. 2000, pp. 410-421.

[4] J.E. Brazy, D.V. Lewis, M.H. Mitnick, and F.F. Jobsis vander Vliet, "Noninvasive Monitoring of Cerebral Oxygenation in Preterm Infants: Preliminary Observations," *Pediatrics*, vol. 25, no. 2, Feb. 1985, pp. 217-225.

[5] J.S. Wyatt, D.T. Delpy, M. Cope, S. Wray, and E.O.R. Reynolds, "Quantification of Cerebral Oxygenation and Haemodynamics in Sick Newborn Infants by Near Infrared Spectroscopy," *Lancet*, vol. 2, no. 8515, Nov. 1986, pp. 1063-1066.

[6] M. Ferrari, E. Zanette, I. Giannini, G. Sideri, C. Fieschi, and A. Carpi, "Effect of Cartid Artery Compression Test on Regional Cerebral Blood Volume, Haemoglobin Oxygen Saturation and Cytochrome-c-oxidase Redox Level in Cerebrovascular Patients," *Adv. Exp. Med. Biol.*, vol. 200, 1986, pp. 213-222.

[7] N.B. Hampson, E.M. Camporesi, B.W. Stolp, R.E. Moon, J.E. Shook, J.A. Griebel, and C.A. Piantadosi, "Cerebral Oxygen Availability by NIR Spectroscopy during Transient Hypoxia in Humans," *J. Appl. Physiol.*, vol. 69, no. 3, Sept. 1990, pp. 907-913.

[8] Y. Hoshi and M. Tamura, "Detection of Dynamic Changes in Cerebral Oxygenation Coupled to Neuronal Function during Mental Work in Man," *Neurosci. Lett.*, vol. 150, no. 1, Feb. 1993, pp. 5-8.

[9] S. Fantini, S.A. Walker, M.A. Franceschini, M. Kaschke, P.M. Schlag, and K.T. Moesta, "Assessment of the Size, Position, and Optical Properties of Breast Tumor in Vivo by Noninvasive Optical Methods," *Appl. Opt.*, vol. 37, no. 10, Apr. 1998, pp. 1982-1989.

[10] H. Jiang, Y. Xu, N. V. Iftimia, J. A. Eggert, K. L. Klove, L. Baron, and L. Fajardo, "Three-dimensional optical tomographic imaging of breast in a human subject," *IEEE Trans. Med. Imaging*, Vol. 20, No. 12, Dec. 1991, pp. 1334-1340.

[11] H. Jiang, N.V. Iftimia, Y. Xu, J.A. Eggert, L.L. Fajardo, and K.L. Klove, "Near-Infrared Optical Imaging of the Breast with Model-Based Reconstruction," *Acad. Radiol.*, vol. 9, no. 2, Feb. 2002, pp. 186-194.

[12] W. Cheong, S.A. Prahl, and A.J. Welch, "A Review of the Optical Properties of Biological Tissues," *IEEE J. Quantum Electron.*, vol. 26, no. 12, Dec. 1990, pp. 2166-2185.

[13] R.A.J. Groenhuis, H.A. Ferwada, and J.J. Ten Bosch, "Scattering and Absorption of Turbid Materials Determined from Reflection Measurements. 1. Theory," *Appl. Opt.*, vol. 22, no. 16, Aug. 1983, pp. 2456-2462; "Scattering and Absorption of Turbid Materials Determined from Reflection Measurements. 2. Measuring Method and Calibration," *Appl. Opt.* vol. 22, no. 16, Aug. 1983, pp. 2463-2467.

[14] T. Nakai, G. Nishimura, K. Yamamoto, and M. Tamura, "Expression of Optical Diffusion Coefficient in High-Absorption Turbid Media," *Phys. Med. Biol.*, vol. 42, no. 12, Dec. 1997, pp.

2541-2549.

[15] M. Bassani, F. Martelli, G. Zaccanti, and D. Contini, "Independence of the Diffusion Coefficient from Absorption: Experimental and Numerical Evidence," *Opt. Lett*., vol. 22, no. 12, June 1997, pp. 853-855.

[16] S.R. Arridge, M. Schweiger, M. Hiraoka, and D.T. Delpy, "A Finite Element Approach for Modeling Photon Transport in Tissue," *Med. Phys*., vol. 20, no. 1, Mar. 1993, pp. 299-309.

[17] K.D. Paulsen and H. Jiang, "Spatially Varying Optical Property Reconstruction Using a Finite Element Diffusion Equation Approximation," *Med. Phys*., vol. 22, no. 6, June 1995, pp. 691-701.

[18] S.R. Arridge, M. Hiraoka, and M. Schweiger, "Statistical Basis for the Determination of Optical Pathlength in Tissue," *Phys. Med. Biol*., vol. 40, no. 9, Sept. 1995, pp. 1539-1558.

[19] G. Vishnoi, A.H. Hielscher, N. Ramanujam, and B. Chance, "Photon Migration through Fetal Head in Utero Using Continuous Wave, Near-Infrared Spectroscopy: Development and Evaluation of Experimental and Numerical Models," *J. Biomed. Opt*., vol. 5, no. 2, Apr. 2000, pp. 163-172.

[20] I. Fridolin, K. Hansson, and L.G. Lindberg, "Optical Non-Invasive Technique for Vessel Imaging: II. A Simplified Photon Diffusion Analysis," *Phys. Med. Biol.*, vol. 45, no. 12, Dec. 2000, pp. 3779-3792.

[21] M. Firbank, S.R. Arridge, M. Schweiger, and D.T. Delpy, "An Investigation of Light Transport through Scattering Bodies with Non-Scattering Regions," *Phys. Med. Biol*., vol. 41, 1996, pp. 767-783.

[22] S.R. Arridge, H. Dehghani, M. Schweiger, and E. Okada, "The Finite Element Model for the Propagation of Light in Scattering Media: a Direct Method for Domains with Nonscattering Regions," *Med. Phys*., vol. 27, 2000, pp. 252-264.

[23] J. Ripoll, M. Nieto-Vesperinas, S.R. Arridge, and H. Dehghani, "Boundary Conditions for Light Propagation in Diffusive Media with Nonscattering Regions," *J. Opt. Soc. Am. A*, vol. 17, no. 9, Sept. 2000, pp. 1671-1681.

[24] E. Okada, M. Firbank, M. Schweiger, S.R. Arridge, M. Cope, and D.T. Delpy, "Theoretical and Experimental Investigation of Near-Infrared Light Propagation in a Model of the Adult Head," *Appl. Opt*., vol. 36, no. 1, Jan. 1997, pp. 21-31.

[25] J. Ripoll and M. Nieto-Vesperinas, "Index Mismatch for Diffuse Photon Density Waves at Both Flat and Rough Diffuse-Diffuse Interfaces," *J. Opt. Soc. Am. A*, vol. 16, no. 8, Aug. 1999, pp. 1947-1957.

[26] H. Dehghani and D.T. Delpy, "Near-Infrared Spectroscopy of the Adult Head: Effect of Scattering and Absorbing Obstructions in the Crebrospinal Fuid Lyer on Lght Dstribution in the Tssue," *Appl. Opt.* vol. 39, no. 25, Sept. 2000, pp. 4721-4729.

[27] P. van der Zee, M. Essenpreis, and D.T. Delpy, "Optical Properties of Brain Tissue," *Photon Migration and Imaging in Random Media and Tissues*, R.R. Alfano and B. Chance, eds., *Proc. SPIE*, vol. 1888, 1993, pp. 454-465.

[28] M. Firbank, M. Hiraoka, M. Essenpreis, and D.T. Delpy, "Measurement of the Optical Properties of the Skull in the Wavelength Range 650-950 nm," *Phys. Med. Biol*., vol. 38, no. 4, Apr. 1993, pp. 503-510.

[29] L.-H. Wang, S.L. Jacques, and L.-Q. Zheng, "MCML – Monte Carlo Modeling of Photon Transport in Multi-Layered Tissues," *Computer Methods and Programs in Biomedicine*, vol. 47, no. 2, Feb. 1995, pp. 131-146.

[30] L.-H. Wang, S.L. Jacques, and L.-Q. Zheng, "CONV – Convolution for Responses to a Finite Diameter Photon Beam Incident on Multi-Layered Tissues," *Computer Methods and Programs in Biomedicine*, vol. 54, no. 3, Nov. 1997, pp. 141-150.

**Seunghwan Kim** received the BS, MS, and PhD degrees in physics from Seoul National University in Seoul, Korea, in 1988, 1990 and 1995. Since 1995, he has been with Electronics and Telecommunications Research Institute (ETRI), Korea, as a Principal Member of Engineering Staff, where he has been engaged in research on the dynamics of biological neurons, noise-induced phase transitions, wearable bio-signal monitoring systems, medical image processing, and optical tomography. His research interests are in ubiquitous healthcare and computer-aided diagnosis.

**Jae Hoon Lee** received the BS, MS, and PhD degrees in physics from Seoul National University in Seoul, Korea, in 1994, 1996 and 2002. Since 2002, he has been with ETRI as a Senior Member of Engineering Staff, where he has been engaged in research on optical tomography. His research interests are in diffused optical tomography.